University of Warwick

MPhys Final Year Project

Evaluation of Magnetic Resonance Imaging for Treatment Planning for Brachytherapy for Cervical Cancer

Author:

Matthew Lougher

0700304

Supervisor:

Adrian Wilson

May 2011

Contents

Abstract

A new phantom was designed and built in order to quantify the spatial distortions produced in images taken by MRI for treatment planning of brachytherapy for cervical cancer. It was found that for a field of view of 30 cm; large enough to incorporate the anatomy required to plan treatment, the distortions were of the order of millimetres or individual pixels. The images were compared to ones taken by CT and it was found that while the MR images have more inherent distortions, they are of a similar magnitude to random fluctuations in CT, and so it was concluded that MR is a viable method of obtaining images for treatment planning, without the need for additional image correction.

1 Overview of Project

Cervical cancer is responsible for over 253,000 deaths each year worldwide; approximately 50% of those that develop the disease. Roughly 1,000 of these deaths are in the UK alone; corresponding to a national mortality rate of 35% [1], and so new methods of planning and carrying out treatment are continually being developed. This project investigates a new method of planning treatment of cervical cancer making use of Magnetic Resonance Imaging (MRI) rather than plane film X-ray images which are conventionally used, or X-ray Computed Tomography (CT) which is starting to be used more for this process. The advantage of MRI is that it is sensitive to variations in soft tissue, and so tumours will be visible on the resulting images, whereas with methods based on X-ray exposure it is hard if not impossible to distinguish tumours from the surrounding tissue. However, MRI images are more susceptible to distortions from the local environment, which must be quantified. In order to do this, the project entails creating a phantom; a model with identifiable key points allowing easier analysis of images taken, and using it to quantify the distortion in the MRI machines of various strengths and styles. The results will then be compared to images of the phantom taken using CT to see how suitable MRI is for the task.

2 Brachytherapy

2.1 Introduction

Brachytherapy (from the Greek "brachio'", meaning short) is a method of radiotherapy involving the insertion of a radioactive source into a patient near to the cancerous area, either temporarily or permanently if the half life is short enough [2], for treatment of tumours in or around body cavities. As the sources are held inside the patient, it is important that they be gamma emitters, as these are high enough energy to pass out of the body depositing only a fraction of their energy in the nearby tissue, whereas an alpha or beta emitter would deposit all of its energy within a very short distance as they are highly ionising. This would result in a greater chance of damage to healthy cells, despite also destroying more cancerous cells, and so a compromise is made in order to preserve the healthy tissue. The source is administered to the patient by passing it into, and then retrieving it from,

an applicator which is inserted into a body cavity in the patient in an operating theatre. The patient is then moved into a shielded treatment room where the source can be handled and inserted without risk to surrounding areas of tissue, or to people in nearby areas.

The placement of the radioactive source in brachytherapy is vital to the overall treatment; due to the general inverse square law that radiation follows (Figure 1) [3], so the applicator is inserted so as to be as close to the affected area as possible. If it is assumed that ideally the source
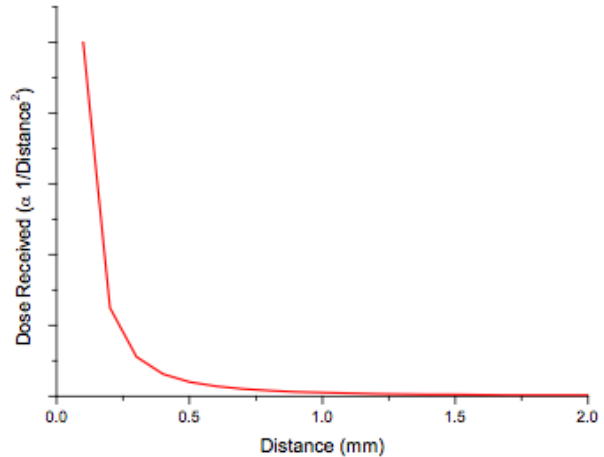

Figure 1: Inverse square relation between dose received and distance from the source. It can easily be seen that a displacement of just 1 mm dramatically reduces the dose received, hence the need for accurately determining the position of the source relative to the tumour.

should be within 5 mm of the tumour, then a variation in its position by as little as 1 mm is enough to reduce the dose received by 30%. The shape of the applicator can be changed in order to minimise the sensitivity of the treatment to position, but its exact position still needs to be known. For this reason, a CT scan, or a series of plane film X-ray images, is traditionally taken of the patient with the applicator in position, and treatment is then planned around the positioning of the applicator relative to the cancerous tissues. Care is also taken during this stage to ensure that radiosensitive areas such as the bladder or rectal wall do not receive harmful amounts of radiation (some applicator designs have built in radiation shields positioned to protect the rectal wall from most of the radiation as this tissue is highly radiosensitive).

2.2   Treatment Systems

There are several different treatment planning methods, each using a different applicator style and identified key points in the body. The Paris Interstitial System, for example, entails inserting radioactive iridium wires directly through the cancerous tissue and leaving them for an amount of time determined by the proximity of the wires to the tumour and each other [2]. In this way, areas that are not near body cavities, e.g. the breast, can be treated with brachytherapy. This system gives an easily regulated dose distribution

centred on the volume created by the iridium wires, and the dose at any point may be calculated from the linear geometry of the system [4].

Another method used is the Manchester System, which will be focused on for this report as it is designed specifically for the treatment of cervical cancer. This system entails inserting an applicator consisting of an intra-uterine tube (IUT) coupled with two ovoids (elongated spheres) into the patient through the vagina [4]; the shape of the applicator (see Figure 2) allows the radiation distribution profile to be accurately determined. There are two different methods of applying the calculated radiation
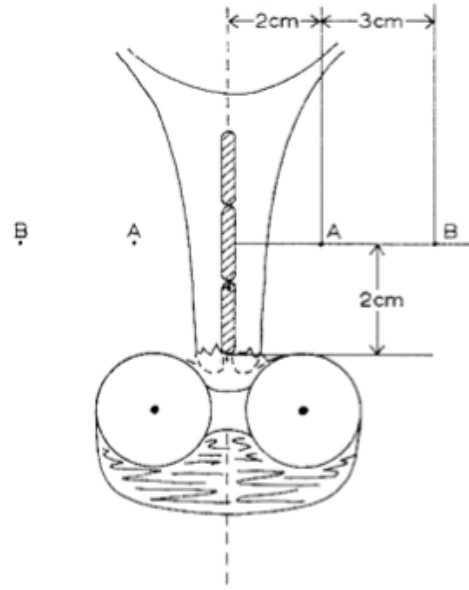
Figure 2: Schematic of a Manchester applicator in situ in a patient, with key points identified [4].

dose through these applicators; so called low dose rate (LDR) and high dose rate (HDR) techniques. LDR delivers the dose through the use of low activity radioactive seeds; by controlling the number and spacing of seeds inserted into the IUT and ovoids, the maximum dose can be delivered to the affected area while minimising the exposure to sensitive areas. HDR, on the other hand, uses a single high activity source on the end of a wire, which inserts and retracts the isotope such that it spends an amount of time at each of several dwell positions inside the applicator as outlined by the treatment plan [5]. The key reference points for calculating dose for both possible methods in this system are labelled in Figure 2 as point A; the point at which the uterine vessels cross the urethra, and point B; the position in the pelvic wall at the same height above the edge of the cervix as point A [4]. Approximate distances are given in Figure 2, but these can vary from patient to patient; which is another reason that images of the patients individual anatomy need to be taken before treatment commences.

Once the applicator is in place and has been imaged, the images are analysed to identify the IUT, ovoids and key structures, such as the bladder and rectal wall. This allows the treatment to be planned, calculating the duration of exposure and the position of source needed to best treat the tumour without damaging nearby healthy tissue. The design of the Manchester system allows the amount of source in each of the ovoids and the IUT to be varied, resulting in what is referred to as the sculpted pear dose distribution [6],

as shown in Figure 3. The shape of this distribution can be further modified by using a variation of the Manchester system, such as the Interstitial Manchester system which has added needles in the ovoids to further modify the dose distribution, or by using other modified versions of the applicator; such as using tandem ovoids (with the ovoids stacked one on top of each other below the IUT) or by using an applicator with a ring around the base of the IUT instead of the ovoids. The applicators can also be modified to be fitted with shielding to further protect sensitive areas.
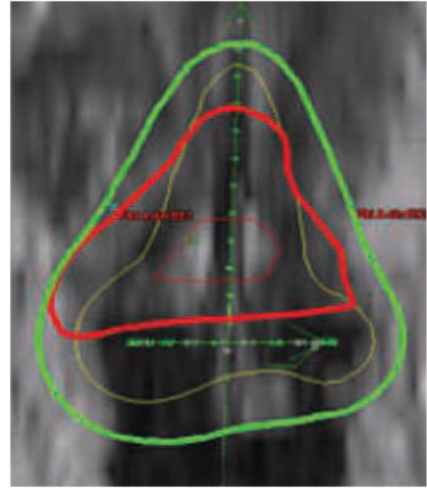

Figure 3: Example of sculpted pear, modified from [7]

2.3 Doses

Previously, the term dose has been used to describe the amount of radiation received by the tissue; by this the absorbed dose is meant, i.e. the amount of energy absorbed per kg of tissue, measured in Grays (Gy). This can then be corrected to take into account the radiosensitivity of the tissue, giving the equivalent dose measured in Sievets (Sv) [8]. For both definitions, the lowest possible dose to healthy tissue is desired while also delivering a high dose to the cancerous cells. As it is hard to identify all tissue types in images, and due to the way the dose is specified, software such as PLATO uses absorbed dose rather than equivalent dose in the calculated treatment plan.

NB: Although both LDR and HDR (explained above) are valid and regularly used methods for brachytherapy, it is most commonly recommended that HDR be used in the treatment of cervical cancer [9], using sources that usually deliver about 1200cGy to the tissue per hour [5].

3 Computed Tomography (CT) Imaging

3.1 Introduction

X-ray Computed Tomography (CT) images are obtained by rotating an X-ray source and a detector around a ring, in the middle of which lies the patient. The intensity of the

beam received by the detector depends on the attenuation due to the tissues the beam passes through; each type of tissue has a linear attenuation coefficient μ, and the intensity of the beam as it passes through a distance x of any medium is given by [10]:

$$I = I_0 e^{-\mu x} \tag{1}$$

And so if the beam passes through multiple different mediums (i.e. multiple tissue types), the intensities sum as follows [10]:

$$I = I_0 e^{-\sum_i \mu_i x_i} \tag{2}$$

In this way, a series of intensities are obtained, with one summation such as (2) per detector position. Images are then reconstructed via a process known as back projection, where the intensities are projected backwards through a matrix of elements (the pixels of the final image), each representing a small area with coefficient μ_i. Through computer algorithms, an image is then built with contrast corresponding to the coefficient of each pixel, and so a slice through the patient can be reconstructed, with internal structures identified by varying the contrast.

Currently, treatment planning is mainly done from plain film X-ray or CT images of the patient once the applicator has been inserted, and although this leads to clear identification of the metallic components of the applicator, the contrast between soft tissues is often very low, as the difference in attenuation of X-rays between different soft tissue types is very small, leading to poor soft tissue delineation [11]. This means that while the applicator position is easy to specify, and the position of some organs such as the bladder can be determined by introducing radiological contrast fluid into the body, the exact position of the tumour is difficult to determine as there is little or no contrast difference between the healthy cervix and any cancerous tissues.

4 Magnetic Resonance Imaging (MRI)

4.1 Introduction

Another method of imaging the anatomy of patients is to use Magnetic Resonance Imaging (MRI), which images the distribution of H^+ ions in the body; mostly found in water

molecules [12]. The principle behind this imaging technique lies in quantum mechanics; each individual atomic nucleus has associated with it a magnetic moment, which either lies parallel or antiparallel to the spin angular momentum of the nucleus, depending on whether the gyromagnetic ratio of the atom, γ, is greater than (parallel) or less than (antiparallel) zero. The magnetic moment, μ (not to be confused with the linear attenuation coefficient defined earlier), is defined as [12]:

$$\mu = \gamma S \tag{3}$$

where S is the spin angular momentum of the nucleus. In a relaxed state, with no external magnetic field, these magnetic moments are ordered completely randomly in most materials; however, when placed in a magnetic field of strength B_0, the magnetic moments begin to precess around the external field direction with a frequency ω, as shown in Figure 4, i.e. the spin angular momentum rotates around an axis aligned with the external field (this is analogous to a spinning top as it starts to slow down; it still spins on its own axis, but is slanted and also starts rotating around a vertical axis). The reason the magnetic moment does not completely align with the external field is due to the
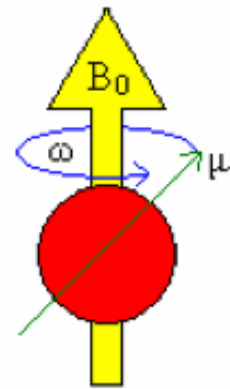

Figure 4: Illustration of spin precession of a nucleus in an external magnetic field.

Heisenburg uncertainty principle, as only the total spin angular momentum and a single component can be known at anyone time, and if the moment were aligned parallel to B_0 (typically taken as the z axis) then the other two components would have to be zero, meaning all components of the spin would be known [13].

The frequency of precession for a specific nucleus in a specified external field is called the Larmor frequency, ω_0, and is calculated form the Larmor equation [14]:

$$\omega_0 = \gamma B_0 \tag{4}$$

By applying a radio frequency (RF) pulse of an additional magnetic field perpendicular to B_0 at the Larmor frequency of hydrogen atoms, any hydrogen atoms in the patient resonate, meaning they absorb energy from the pulse and fall into phase alignment with each other.

Their precession also changes alignment to lie 90° from the direction of B_0. Once the RF pulse has been removed, the signal in the receiver coil decreases due to a process called Free Induction Decay (FID), so called as it is the decay of the induced signal in the absence of the RF field [14]. A receiver coil placed around the patient detects this transitioning of the spins as a magnetic resonance (MR) signal.

The signal varies depending on the chemical situation of the hydrogen atoms; for instance water molecules contain hydrogen atoms bonded to oxygen, which are small and light molecules, and so have a higher initial energy, and dont absorb the resonance energy very efficiently, and so have a long relaxation time [14]. The differences in relaxation time between different media give a difference in contrast on the image, and so by altering the time scale of the experiment you can change how different media appear. For instance, a T1 weighted image shows water as dark whereas a T2 weighted image shows it as light, as both its T1 and T2 times are long (where T1 and T2 are labels given to relaxation times for energy being transferred from the nucleus to the surrounding lattice or other nuclei respectively) [14].

4.2 Distortion Effects

One of the main problems with MRI is that the images are subject to distortions on the order of up to a centimetre [15], which must be corrected if they are to be used for work where anatomical measurements are required to high precision such as brachytherapy treatment planning, where as previously stated locations must be determined to within millimetres. Inhomogeneities in the external field B_0 are responsible for many of the distortions; as they change the strength of the field locally, so instead of the field in (4) being B_0, it would be $(B_0 \pm \delta B)$, where δB is a small change in the field strength. This would then affect the precession frequency of hydrogen atoms in these areas and lead to incoherence in the atomic spins. As position is determined by this precession frequency, any local variations lead to distortions in the image. This can be minimised by the use of pulse sequences [14], which reset the spins and bring them back in phase with each other, restoring cohesion. One pulse sequence often used is a spin echo pulse sequence, where the decay of cohesion due to inhomogeneities is reversed by flipping the spins by 180°, so that whereas the spins were previously diverging, they now converge back to cohesion [12].

Another source of distortion (and a cause of inho-mogeneities) is due to the edge effects of the magnet used. For most of the initial work in this project, an open scanner will be used, which is one that has two separate permanent magnets held apart with a gap between them sufficient enough for a patient to fit in (as opposed to a closed scanner where a cylindrical electromagnet is used, and the patient goes inside the centre of the cylinder). As the magnet is not infinite,
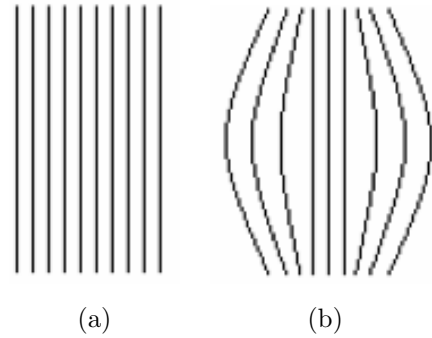

(a)   (b)

Figure 5: (Exaggerated) Illustration of field distortion due to edge effects of the magnet.

instead of a regular, idealised field such as illustrated in Figure 5a, the field is stretched around its edges as in Figure 5b, leading to a ballooning of the images away from the centre of the field. Quantifying this distortion is one of the aims of this project, with the intention of being able to correct it by bringing the image back to be 'square if necessary. Note that this distortion will still be there in images from closed scanners, but will be much reduced as the field lines are focused in that case by the solenoidal shape of the magnet.

4.3   Comparison with CT for Treatment Planning

The main advantage of MRI over CT for brachytherapy treatment planning is the fact that MRI is very good at soft tissue delineation [11], meaning that different soft tissues are easily identifiable, and that cancerous cells can be differentiated from healthy tissues [16]. Coupled with this is the fact that CT scans use ionising radiation while MRI does not, although this is a minor amount compared to the dose received by the treatment. However, it is still an exposure to ionising radiation, and becomes more relevant if multiple images need to be taken. However, MRI doesnt inherently contain information about tissue electron densities, which are needed to calculate absorbed dose distribution [17] and there could also be problems if the patient has any metallic (especially ferromagnetic) implants/pacemaker, or is larger than average size, as the larger the patient is, the more the distortions become apparent [18].

One compromise is to use fusion images, which use both MRI and CT image in tandem to be able to locate the tumour with ease on the MR image and map it onto the undistorted CT image. However, this technique is still flawed as there are variations between the fusion

techniques for different patients, depending on their size [18], and also the patient is still exposed to X-rays, so one advantage of using MRI is negated.

5   Phantom

One of the main experimental tools for assessing medical imaging processes is the phantom, which is a physical representation of the patient. The design of the phantom varies depending on the purpose of the investigation; some are simply Perspex boxes filled with water, whereas others can be more complicated. Although it is true that using a phantom reduces the number of errors normally associated with boundaries between regions of differing magnetic susceptibility, these are normally quite small within the patient, and it is in fact the main boundary between the patient and the air that produces the most errors, which of course the phantom is able to simulate. One of the most common phantom designs is to have an internal Perspex sheet with a grid of holes at set distances apart, allowing the distance between the holes on the image to be compared to the known distance [19].

5.1   Phantom Design

In designing the phantom for this project, several things had to be taken into account:

1. How to include reference points that would be picked up by the scanner, so as to be able to map distortions.

2. How to simulate the distortions added to images by the applicator, as images of the patient would be taken with the applicator in situ, so any effects this will have on the image must be represented.

3. How long it would take to make, as our time using the MRI machines in the hospital was limited to times when they were not being used for patients.

4. Its final overall size, so it could fit in any of the three MRI machines available for use in this project.

   The first step in the design process was to determine the size of the phantom. As a preliminary test, a large Perspex box was part filled with water and an applicator was

placed in the bottom of it with its ends covered in cling-film and tape in order to keep water from getting inside the applicator, which, according to the radiographer we worked with, could leave a residue that could cause clogs to form in the applicator. An image taken of this set up, using a generic body coil as the receiver can be seen in Figure 6. It is evident that there are high distortions in this image, and it was established that the vertical line artefacts were
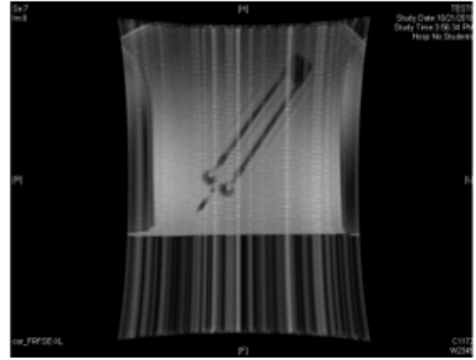

Figure 6: Preliminary image taken of an applicator in a tank of water.

a result of the amount of air that was present between the top of the water and the top of the tank. Therefore it was realised that our phantom would need to be built such that it filled the coil, minimising the amount of air present. It was also decided that a CTL (cervical, thoracic, lumbar) coil would be used instead of the body coil, as it is rigid and so the phantom could more easily fit the same for each measurement, whereas the flexible body coil could easily be positioned differently on the phantom for each experiment. This set a maximum size of $24 \times 24 \times 24$ cm for our phantom in order for it to fit in this coil.

It was decided that our phantom should be made of 10 mm thick Perspex sheets, as it is readily available, strong and inexpensive, and filled with water with a contrast solution mixed in to enhance the images obtained. A shape was chosen that was wider at the base than it was at the top, for stability, with sloping sides to allow maximum height while the narrow top ensured it would fit inside the curve of the CTL coil. Inside the phantom were two horizontal and two vertical grids of holes from which the main image analysis would
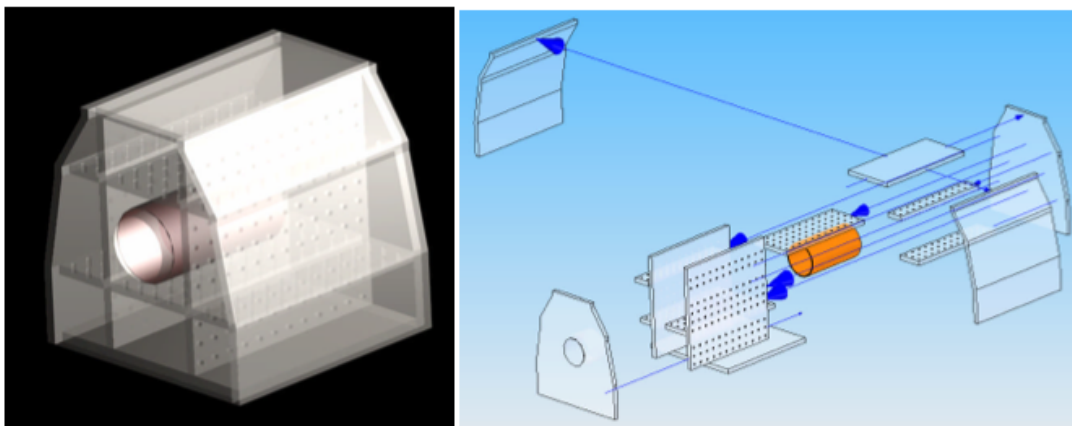

Figure 7: CAD rendered and exploded images of the planned phantom, illustrating the separate parts required to build it.

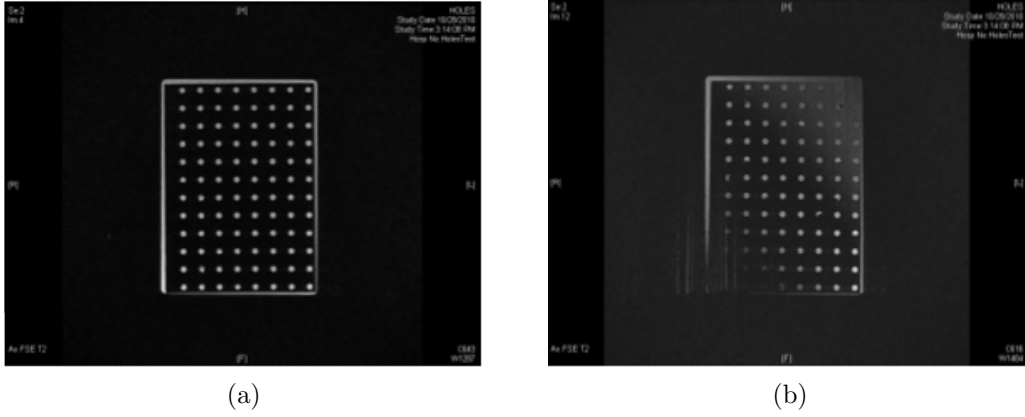(a)   (b)

Figure 8: Shows images taken through the Perspex sheets with holes a) drilled all the way through and b) drilled half way through.

be done. The applicator was accommodated for by inserting a plastic tube into one face of the phantom with a rubber 'sock extending from its end, into which the applicator could be placed without it getting wet. The pressure of the water above the sock would mould it around the applicator, forcing any air out through the hole in the end, so reducing the amount of air in the phantom while allowing the applicator to be removed easily. A CAD rendition of the proposed phantom, along with an exploded diagram of it, can be seen in Figure 7. In order to make the phantom more efficient to use, it was planned that it should be split into three water tight compartments; one on either side which could be left filled and one in the centre that would be filled and emptied each time as the applicator is inserted or removed (due to the cost of the applicators, it was impossible to incorporate one into the design permanently). In order to do this, the vertical grids werent drilled all the way through, but instead had holes which went 5 mm deep into the Perspex. This idea was first tested on a smaller scale, with two sheets of Perspex being prepared individually; one with the holes drilled all the way through, and one with holes drilled only half way. These were each placed in a small Perspex box already in the MRI room and an image slice was taken through each, which can be seen in Figure 8. As can be seen, the holes appear just as clear in each case, although in the image taken of the grid with part drilled holes it can be seen that a few of them still have air bubbles trapped in them, meaning we would have to be careful when filling the side sections. The diagonal gradient evident on Figure8b was caused by the Perspex not lying flat inside the small box, illustrating the need for the planes in our phantom to be precisely aligned with the imaging planes of the scanners.

5.2 Phantom Modifications

Figure 9 shows a photo of the phantom after the initial build period (about 2 weeks). In addition to the details shown on the design, the top piece and upper grid in the central region were designed to be removable for maintenance purposes, in case the rubber sock slipped off and needed putting back on for example. Drainage plugs were also added to either side compartment and to the top for ease of filling/emptying. For the rubber sock, the engineer at the hospital used a rubber glove cut below the
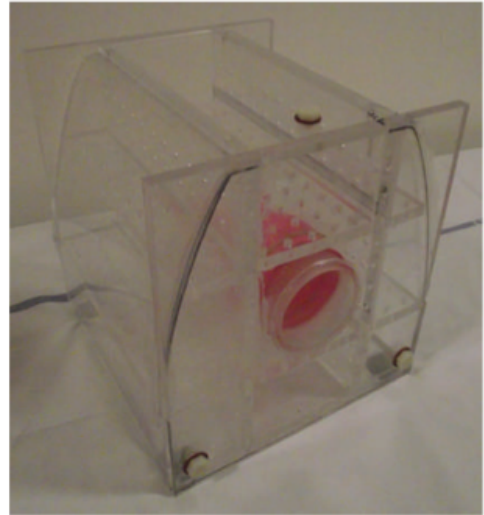

Figure 9: A photo of the empty phantom.

thumb and sealed shut, giving a strong yet flexible rubber tube as required. Due to the inclusion of this glove, the phantom was christened 'Marigold, which is the name that would be used to identify it on the MRI imaging software later.

Upon testing the phantom, it was found that there were several leaks; one internal allowing water to seep from the left hand compartment (with the face with the hole in being identified as the front) into the central chamber, and one external leak allowing water to escape from the right hand compartment out of the phantom completely.

Also during testing, it was found that the planned use of water pressure to squeeze the rubber tube around the applicator worked too well, and if the applicator was let go once the central chamber was full, it shot out of the phantom completely. It was

also found that the glove had torn slightly and needed replacing, validating the requirement that the lid and upper grid be removable. The phantom was then emptied and sent back to the engineers with the request that they design a Perspex clamp to sit on the front of the phantom and hold the applicator in, along with details of the leaks that needed fixing. Figure 10 shows a photo of the modified phantom with the applicator in and full of water. It can be
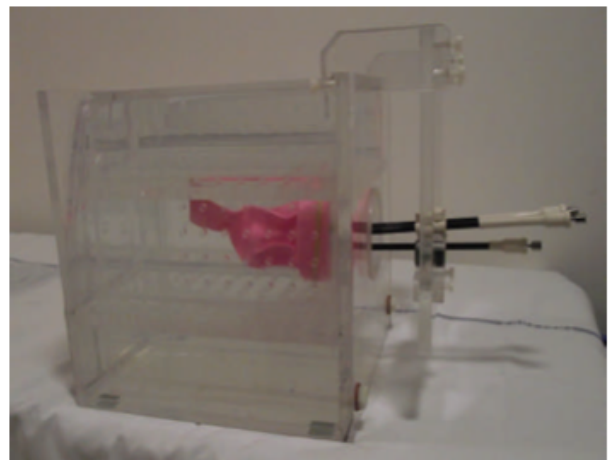

Figure 10: A photo of the modified phantom full of water.

seen in the photo how the rubber tube shrinks to fit around the applicator as designed.

Throughout the course of the project, several more leaks developed in the phantom, although all were minor and easily fixed. Other modifications to the original design include the addition of a lip around the inside of the top of the central chamber upon which the top lid sits, which then had silicon grease applied to it in order to form a water tight seal when the lip was screwed down (using plastic screws). Also, a pair or ridges were added to the hard plastic tube that the rubber tube stretches over. These were spaced such that elastic bands fitted neatly between them, allowing a better seal to prevent water from leaking out through the tube. With this final addition, the phantom was completed, and images could be taken to be analysed.

6 Experimental Method

6.1 Applicator

The applicator used for this project was a Utrecht Interstitial Fletcher CT/MR Applicator [20]. This is a variation on the Fletcher applicator (which itself is a MR compatible variation of the Manchester applicator mentioned in section 2.2) which allows for the use of interstitial needles to be fitted into the ovoids for the

Figure 11: A photo of the Utrecht Interstitial Fletcher CT/MR Applicator used.

treatment of more developed cancer which would otherwise require the source to be left at dwell positions for times long enough to damage sensitive normal tissues in the area. The needles were not inserted into the applicator for our experiments as the majority of cases dont need them, although the applicator set did include a set of MR safe needles.

As mentioned, this applicator is completely MR compatible, meaning it is made entirely of plastic and other non-metallic materials. Some companies offer titanium applicators which, while being non-magnetic and therefore wouldnt be dangerous to use in MRI, are still metal and so would result in large local distortions on the image. A photo of the applicator used can be seen in Figure 11.

6.2 MRI Machines

For the majority of the project; including all of the preliminary work mentioned so far, the MRI machine used was a 0.35 T GE Ovation open scanner, which used the CTL receiver coil previously mentioned. In order to experiment across a range of field strengths, we also had access to a 1.5 T Siemens Symphony and a 3 T GE HDxt machine; each of which are closed machines; the more traditional design for MRI scanners. When using the closed scanners, we used a generic body coil as the narrow size of the bore of the scanners didnt allow for large receiver coils to be used.

6.3 Experimental Set Up

To improve the contrast of images taken by all three scanners, the phantom was filled with a solution of gadolinium based contrast enhancer. The solution used was Multihance® Gadobenate Dimeglumine at a ratio of 0.2 ml/kg of water, as instructed by the leaflet supplied with the solution, substituting water for the patients body.

Figure 12: Illustration of the planes traditionally imaged [21].

When scanning the phantom, we followed the established protocol of scanning in the axial, sagittal and coronal planes, as illustrated in Figure 12. In this way, axial scans go from front to back; coronal from bottom to top and sagittal from left to right if the phantom is orientated such that the face with the hole for the applicator (i.e. the front) is taken to point towards the feet of the 'patient lying on their back.

All three MRI machines use a laser crosshair to align the patient centrally within the magnetic field. Each time the phantom was taken into the machine, it was ensured that the crosshair from the laser lined up with the centre of the phantom, which itself was positioned centrally within the receiver coil with the aim of fixing the position of the centre of the magnetic field (where distortions should be minimal) to the centre of the phantom.
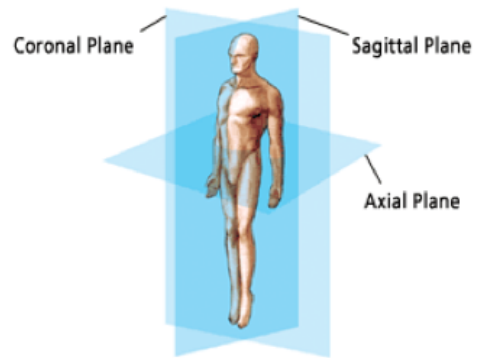
6.4 Analysis Method

It was decided that the best way to track the distortion across the phantom was to use the centre of each hole as a key point, and to measure the deviation from their expected position. To do this, a full size grid of holes was created in Adobe Photoshop for each plane, which was then resized to have the same number of pixels per millimetre as the images. The centre of each hole was identified by eye, as after initially attempting to use the inbuilt edge detection algorithm in ImageJ, plus an extra plugin called FeatureJ, both were deemed unreliable as some of the features we were investigating were less than 5 pixels across. If it was decided that no individual pixel lay in the centre of the hole, then the pixels either side of the centre were highlighted; allowing sub-pixel accuracy and reducing the error in the location of the centre of the hole to a quarter of a pixel in each direction, corresponding to approximately 0.25 mm on average (the exact value depending on the resolution of the image). The same method was applied to the images from the MRI machine, and the image of ideal hole positions was overlaid on the scanned image using ImageJ. The translation from where the centre of the hole should be to where it was on the image was then measured for each hole by counting the number of pixels horizontally and
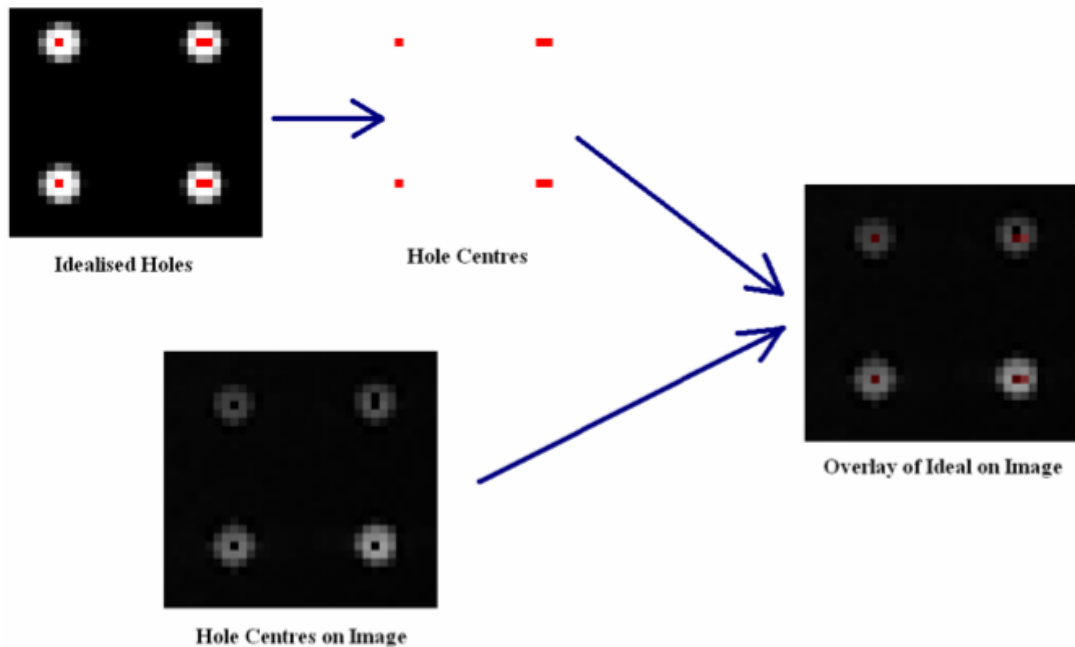

Figure 13: Demonstration of the measurement of hole-centre displacement. Using this extract of 4 holes as an example, hole 1 (top left) has a displacement of $(0, 0)$; hole 2 (top right) has a displacement of $(-\frac{1}{2}, \frac{1}{2})$; hole 3 (bottom left) has a displacement of $(0, 0)$ and hole 4 (bottom right) has a displacement of $(0, -\frac{1}{2})$.

vertically between the two positions, using the convention usually attributed to images where the origin is in the top left corner of the image (i.e. x increases from left to right and y increases from top to bottom). Holes were identified by numbering; with number 1 being the top left corner; increasing across the columns, then continuing at the left hand side of the next row down. An example of this process can be seen in Figure 13.

The distances in pixels measured from each image were then scaled to give displacement in millimetres according to the resolution of the image, and these displacements were organised into matrices, then plotted first as surface maps in Matlab with the x and y axes corresponding to hole number and the distance (i.e. $\sqrt{x^2 + y^2}$) plotted on the z axis. Contour maps were then also made to allow the magnitude of distortion to be categorised easily into 0.5 mm increments, allowing areas of low distortion to be identified at a glance.

6.5   Experimental Sources of Distortion

It was realised that the experimental procedure could add distortions to our images in three ways; from the applicator, from the phantom, and through human interpretation.

Extra distortions added by the applicator could be quantified by taking scans with and without the applicator in and comparing the results; this would test whether the applicator was indeed MR compatible, as it was designed not to introduce extra distortions. However, distortions from the phantom and from human error were harder to calculate.

In order to calculate error due to human interpretation (incorporating the quarter of a pixel error in locating the centre of the holes mentioned previously), an MR image was chosen at random and was analysed independently by both partners taking part in this project. The resulting matrices were then subtracted from one another and a mean was taken, giving an approximate value for the human error associated with the analysis process. The same was then done with an image taken on a CT machine, with the difference between the two approximations of human error quantifying the added distortion due to the presence of the phantom. This method assumes that the phantom does not distort the CT images in any way, whereas in MR the boundary between different magnetic susceptibilities can modify the filed slightly. This problem is exaggerated in our case as the phantom has stark boundaries between air, Perspex and water, whereas in the body the only major boundary is that from air to the body (as magnetic susceptibilities

of different tissues are very similar; differing by at most 2×10^{-6} [22]), which can be smoothed by using a dielectric pad. Hence; extra distortions are added to MR images by our phantom, but not to CT images.

7   Results & Discussion

7.1   0.35 Tesla Machine

The initial scans taken on the 0.35 T machine were done with frequency and phase both set to 256, giving an image with 256 square pixels in each direction. This gave a scan time of approximately 10 minutes, which is a realistic amount of time for a patient to be scanned. The field of view was initially set to 40cm, so the phantom filled just over half the image. It was realised that due to the field bending mentioned earlier (see Figure 5), images taken of the grids in the sagittal plane were too heavily distorted to analyse, as large parts of the grids were
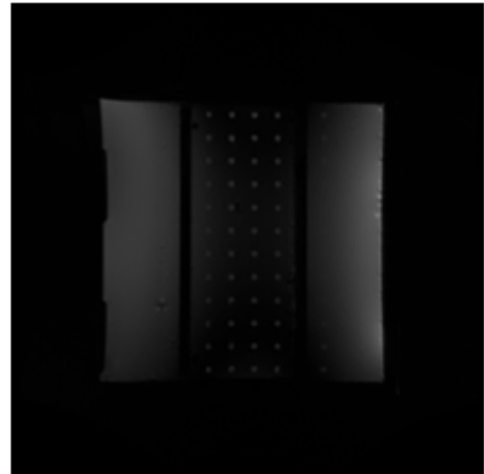

Figure 14: Example of image of one of the sagittal grids with holes missing.

missing due to the holes only being 5 mm deep, so there were easily missed by the image slice, as shown in Figure 14. Also, it was realised that the phantom had insufficient holes in the axial plane to analyse fully, which was an oversight during the design process; thus the main results obtained were of the coronal grids.
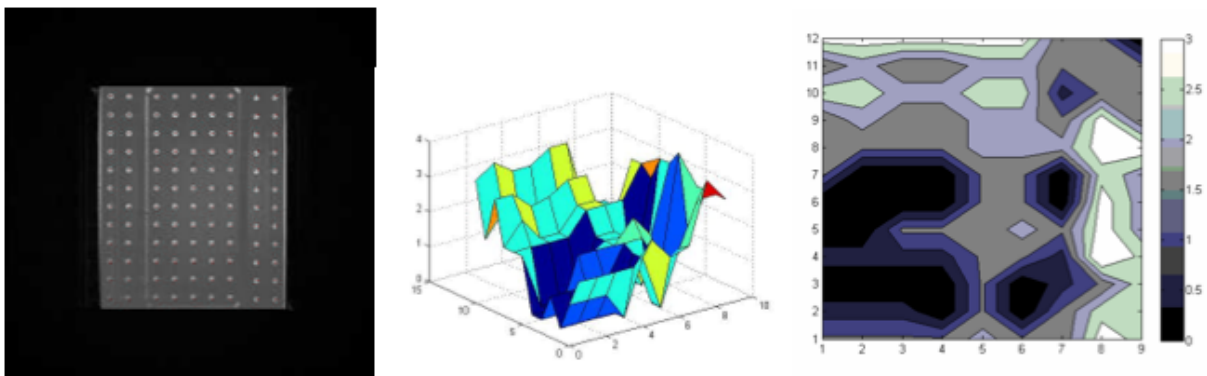

Figure 15: Analysed image of the upper coronal grid. The surface and contour plots show the distortion in millimetres as a function of hole number; hence demonstrating how the distortions vary with position.

17

Figure 15 shows an image taken of the upper coronal grid, along with a surface map and contour map of the distortions. It can be seen that there is a minimum in one corner of the plane, with distortions becoming as high as 3 mm towards the edges. However, it should be noticed that the majority of the distortions are less than 1.5 mm, a result which was also evident in the lower coronal image. In order to focus more on the phantom itself, and improve the resolution of the image, a series of images was taken with the field of view reduced

Figure 16: Lower coronal image taken with field of view set to 20 cm.

to 20 cm; an example of which can be seen in Figure 16. It became apparent that this field of view led to echoes and edge effects during the image reconstruction process, and so despite the increase in resolution, it was decided that a compromise of a field of view of 30 cm would be best. This value was then used for all following MR images, meaning each pixel corresponds to a distance of 1.17 mm.
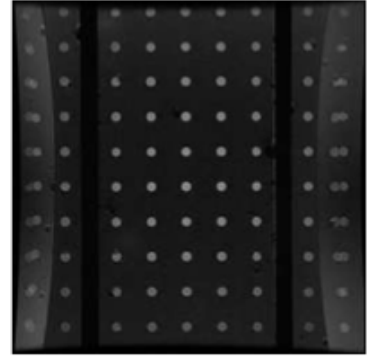
Figure 17 shows an analysis of both the upper and lower coronal planes for the new field of view. It can be seen that the increase in resolution has reduced the average distortion; most now being of the order 1 mm or less. The distortion field also appears more structured; with a single set minimum and the distortions generally increasing with distance from the minimum. It is intriguing that the minimum in the upper plane doesnt lay above the minimum in the lower plane; demonstrating that the phantom wasnt placed perfectly within
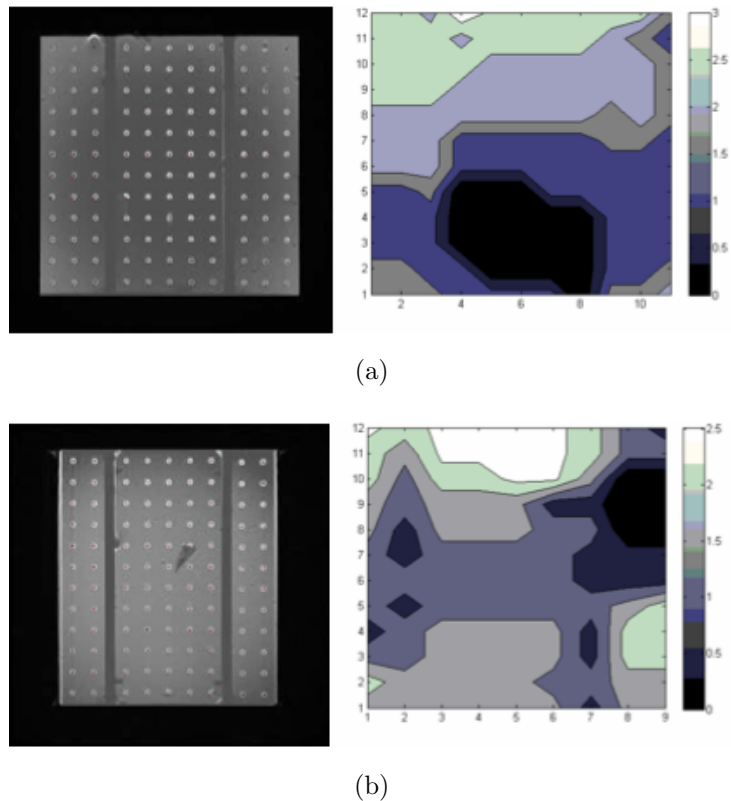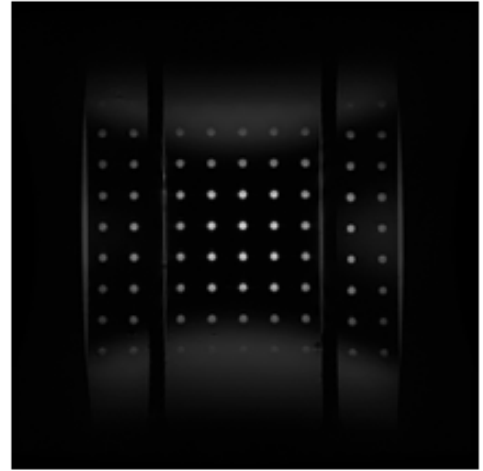

(a)

(b)

Figure 17: Analysis images and plot of the a) lower and b) upper coronal planes with a field of view of 30 cm.

7.2 3 Tesla Machine

With the sale of the open scanner to another hospital, our work then progressed onto the 3 T closed machine, as it was easier to get time booked on this machine than the 1.5 T one. The same phase, frequency and field of view were used, and a full image sequence was taken. Once again, the sagittal images were too heavily distorted to be of use, on top of which the upper coronal plane was highly distorted as well, as illustrated in Figure 18. This is because the bore of the 3 T machine is very narrow, and the upper coronal grid was very near the top of

Figure 18: Heavily distorted upper coronal image.

the bore, where distortions were strongest. Coincidentally, the lower coronal plane lay almost across the centre of the bore, and so had minimal distortions, while corresponding to the approximate position within the bore that would be occupied by the area of interest within a patient. Figure **??** shows the contour maps of the distortions in the two coronal planes. It can be seen that the maximum distortion is a lot lower than in the open scanner, as expected. The mean distortion is 0.9929 mm for the lower coronal and 1.1273 mm for the upper coronal, corresponding to approximately a pixel in each case, although the upper coronal has more holes which arent visible (for the purpose of matrix analysis of the hole distortions, those holes that werent visible had a value of -1 assigned to them, hence they arent apparent on the contour map).
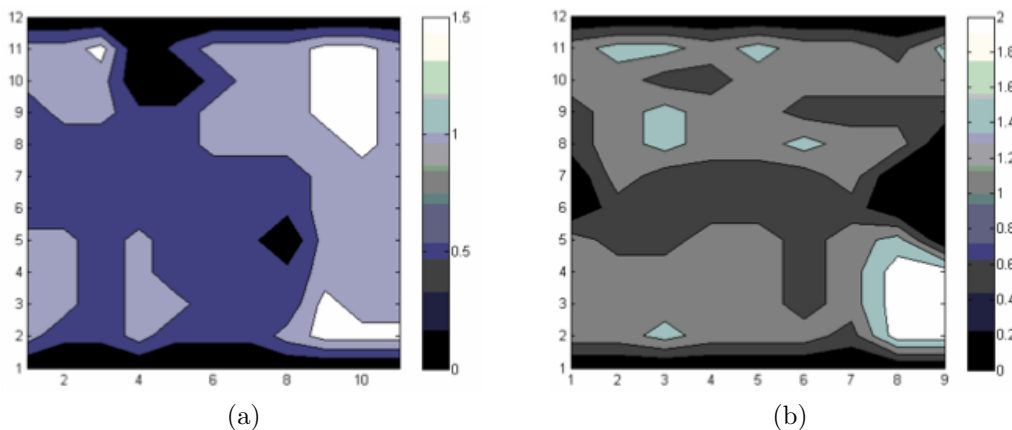

(a)

(b)

Figure 19: Contour plot of distortions in the a) lower coronal and b) upper coronal planes.

7.3   1.5 Tesla Machine

When using this machine, we were surprised to find that the sagittal images were clean enough to be able to analyse, and there were also no holes missing from the upper coronal plane. This was because the bore of the 1.5 T machine is a lot wider than the 3 T scanner, and so the field is homogeneous through a larger volume in the centre of the bore. Figure 20 shows the plots made from all 4 grids of holes. As can be seen, the areas of minimum distortion are very large for the coronal planes, and smaller for the sagittal planes. The mean distortions are 0.9396 mm and 1.3490 mm for the left and right sagittal planes respectively, and 0.6277 mm and 1.1059 mm for the lower and upper coronal planes; as with the 3 T machine these mean distortions across the field correspond to approximately a single pixel or less.

One thing to note is that the 1.5 T scanner is based on different software, and incorporates an extrapolation algorithm which increases the resolution of images to 512×512
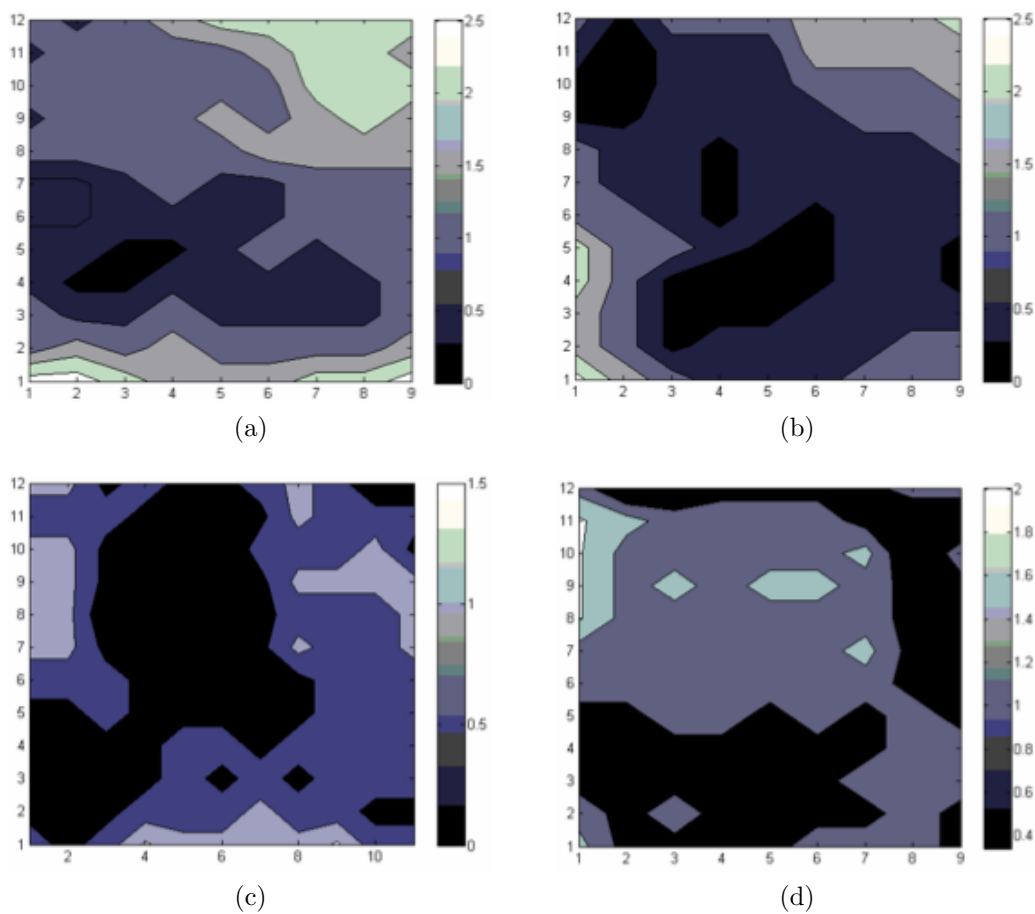

Figure 20: Contour plots of the a) left sagittal, b) right sagittal, c) lower coronal and d) upper coronal planes, taken in the 1.5 T scanner.
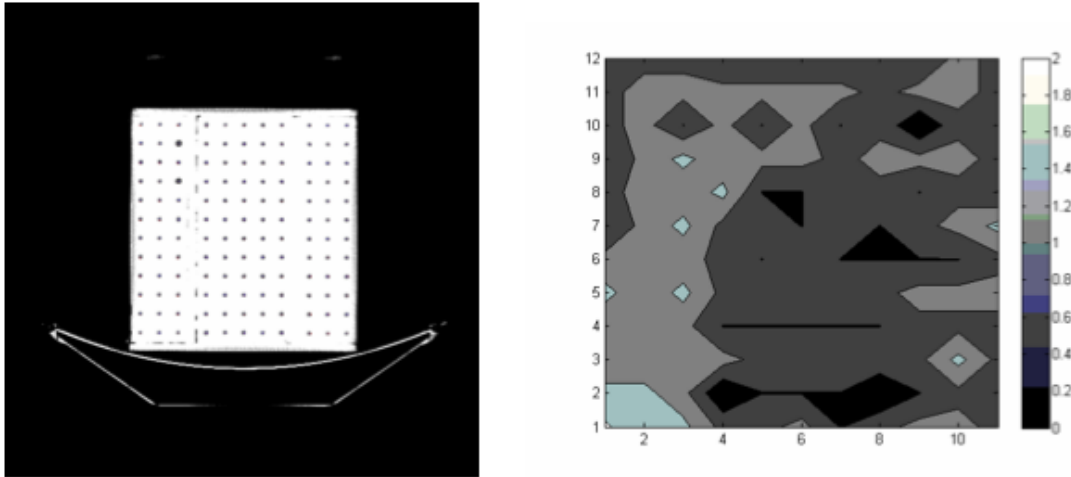
Figure 21: Lower coronal image taken by CT, along with contour plot of distortions.

pixels. It was decided that as this is the setting that would be used for patient scans, it would be appropriate to use these higher resolution images, rather than introduce more errors by attempting to interpolate them back down to be 256×256.

7.4 CT Images

A full series of images of the phantom were taken using one of the CT scanners in the hospital. Due to the restrictions in the software, the field of view was set to 50 cm and the images taken were 512×512 pixels. This means that the pixel size was equivalent to a 25 cm field of view at 256×256 pixels, and so is comparable to the resolution of the MR images taken. Figure 21 shows an example image taken by CT.

As expected, the distortions in the CT images appeared to be random, and were on average less than 1 mm.

7.5 Comparisons

The matrices containing hole distortions from CT were subtracted from those for MR, and the results plotted as contours as before. All of these plots showed very little difference between the two methods; with very few showing deviations of more than 1 mm. Also, there was no bias towards positive or negative values on the most part; indicating that
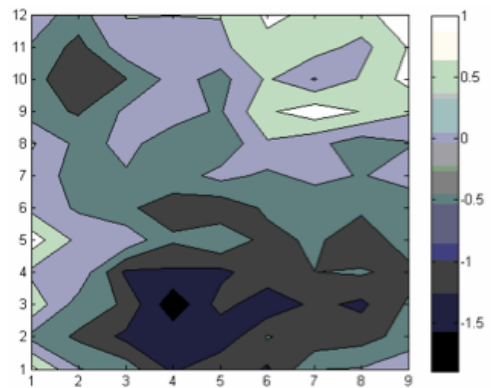

Figure 22: Difference between MR distortion and CT distortion for the left sagittal plane.

there were just as many holes for which the MR was more accurate as there were for which the CT was more accurate. This implies that while the MR images typically have lower distortions near the centre of the field, their magnitude is comparable to the random fluctuations seen in CT images, and so the overall distortion is similar for the two cases. Figure 22 shows an example of a comparison plot between CT and MR for the left sagittal plane.

Figure 23 shows a graph of how the maximum distortion changes between the different machines. The values plotted labelled Max are the mean values of data points within the contour of highest distortion for the two coronal planes for each machine, and the values labelled Mean are the mean values of the whole distortion map. The errors are the standard deviation of the relevant data set.
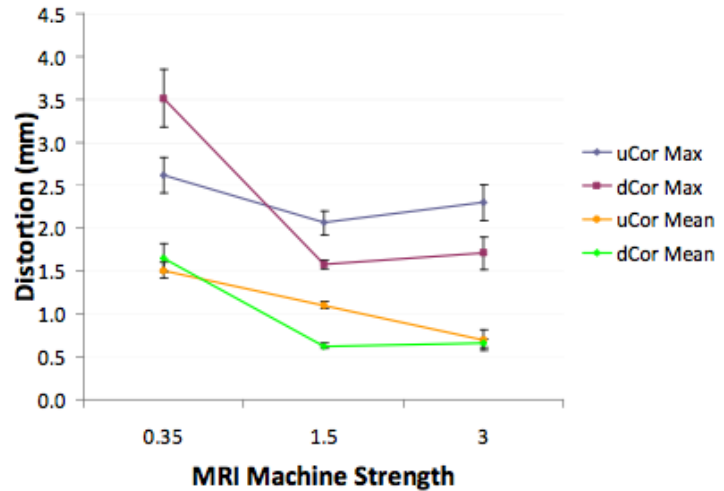

Figure 23: Plot of how distortions vary with increasing field strength. Series labelled uCor are the upper coronal plane, and those labelled dCor are the lower coronal plane.

As can be seen, the 0.35 T machine has the highest maximum and mean distortions, but while the mean distortion generally decreases with field strength, the maximum is much higher for the 3 T machine than the 1.5 T machine. This is likely because the stronger field means that distortions are amplified, so even if the average is lower, the maximum will be higher.

7.6 Errors

As previously explained, there are three main sources of additional distortion to the images as well as the field inhomogeneities; systematic errors due to both the presence of the phantom and applicator, and human error. These were calculated in the previously explained ways, and it was found that the human error for the CT images was 0.0517 mm, whereas for the MR images it was 0.6194 mm. These values are the means of the contour maps show in Figure 24, and give a systematic error due to the presence of the phantom to be 0.5677 mm.
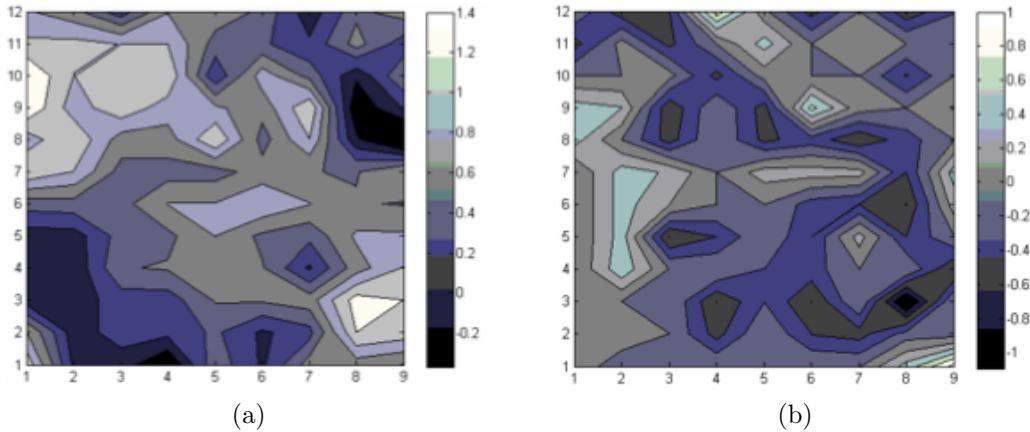
Figure 24: Contour plots approximating the human error in a) MR and b) CT.

A different systematic error according to the presence of the applicator was calculated for each plane for the 1.5 T, 3 T and CT machines; due to the premature sale of the 0.35 T machine we didnt get chance to take a series of images without the applicator in. The average systematic distortion added by the applicator was 0.073 ± 0.050 mm for the 1.5 T scanner, 0.139 ± 0.100 mm for the 3 T scanner and 0.041 ± 0.040 for the CT machine. The errors on these values are the standard deviation of the values calculated for each plane, and so are large as they are calculated from only 4 values. These values lead to the conclusion that the distortions introduced by the applicator are very small, as one would expect from an applicator specifically designed for use in MRI.

7.7   Treatment Plans

The final part of the analysis of the results was to use the Oncentra software to produce a treatment plan from one of the MR image sets and compare it to one made from the CT image set. The images taken on the 1.5 T machine were chosen as they offered the choice of basing the treatment plan either on the coronal or sagittal plane. In order to reduce human errors in the treatment planning method, this stage was carried out by one of the radiographers at the hospital using our images. Unfortunately, due to a health issue with the collaborator from the hospital, this work was not completed and so we have no final answer as to whether the same treatment plan would be produced from the two sets of images. However, we do know that it is possible to use the software to draw up a treatment plan using the MR images, but that it is more difficult due to the lack of markers within the applicator, as CT images are done with metallic markers placed

inside the applicator to highlight dwell positions, which obviously cannot be used in MR images.

8 Conclusions & Recommended Further Work

From all the images analysed (a total of 30 images across all machines), it can be concluded that while MR does have inherent distortions due to inhomogeneities in the magnetic field, they are of the order of magnitude of 1 mm on average, which is not only comparable to average random distortions in CT but is also on the scale of a single pixel for a typical MRI set up. Also, it has been shown that the phantom used introduces significant distortions itself, and so the actual distortions when scanning a patient will be reduced. Due to this, it can be concluded that despite the inherent distortions, MR is a viable alternative to CT, as variations between the images and real life positions appear to be around the 1 mm limit for brachytherapy treatment planning. However, the final test will come once treatment plans for the two methods have been thoroughly compared to see if the same dose distribution is recommended from each image set.

Apart from completing the treatment plan comparison, further work would be to modify/rebuild the phantom such that it has a grid of holes in the axial plane; possibly towards the back between the end of the applicator and the edge of the phantom. Also, as the lack of clarity on the sagittal images is at least in part due to the holes being shallower, they should be drilled deeper such that they are, for example, 0.8 mm deep. This will keep the sides as separate compartments for ease of filling/emptying while also improving the image quality for those grids. Another modification to the phantom would be to decrease the separation between the holes, allowing a more detailed analysis of the distortions by fitting more reference points in each image. It would not be advisable to make the holes smaller in diameter as that would reduce their clarity in the images; as it is most holes were less than 8 pixels across with the field of view set to 30 cm.

It would be possible to increase the phase and frequency such that all images were taken at 512×512 resolution or higher, so as to increase the accuracy of the analysis, but these images would not be as relevant, as they would take too long to obtain compared to the scan time of a patient, and so would be of a greater accuracy than realistically possible.

References

[1] E. Norwitz, J. Schorge, *Obstetrics and Gynecology at a Glance, 3rd Edition*, (Blackwell Publishing, Oxford, 2010)

[2] W. Hendee, G. Ibbott, E. Hendee, *Radiation Therapy Physics, 3rd Edition*, (Jon Wiley & Sons Inc., New Jersey, 2005)

[3] F. Spiers, British Journal of Radiology, **14**, 147-156 (1941)

[4] J. Patterson, *Radium Dosage: The Manchester System*, (E & S Livingstone, Edinburgh, 1967)

[5] C. Yarbro, D. Wujcik, B. Holmes Gobel, *Cancer Nursing: Principles and Practice 7th Edition*, (Jones & Bartlett, Sudbury, 2010)

[6] B. Erickson, Brachytherapy, **2**, 189-199 (2003)

[7] R. Ptter et al., Acta Oncologica, **47**, 1325-1336 (2008)

[8] Bureau International des Poids et Measures, *The International System of Units, 8th Edition*, 2008

[9] S. Nag et al., International Journal of Oncology, **48**, 201-211 (2000)

[10] J. Hseigh, *Computed Tomography: Principles, Design, Artifacts, and Recent Advances*, (SPIE Press, Washington, 2003)

[11] F. Lucente, G. Har-El, *Essentials of Otolaryngology*, (Lippincott, Williams & Wilkins, Philadelphia, 2004)

[12] M. Levitt, *Spin Dynamics*, (John Wilwy & Sons Ltd., Chichester, 2005)

[13] A. Rae, *Quantum Mechanics, 5th Edition*, (CRC Press, Florida, 2007)

[14] C. Westbrook, *MRI at a Glance*, (Blackwell Science Ltd., Oxford, 2002)

[15] J. Aubrey et al, Brachytherapy, **9**, 266-273 (2010)

[16] R. Reznek, A. Saholev, British Journal of Radiology, **78**, S73-S85 (2005)

[17] B. Petersch et al., Radiotherapy & Oncology, **71**, 55-64 (2004)

[18] Z. Chen et al., Physics in Medicine & Biology, **51**, 1393-1403 (2006)

[19] D. Wang, D. Doddrell, Current Medical Imaging Reviews, **1**, 49-60 (2005)

[20] Nucletron Utrecht Interstitial Fletcher CT/MR Applicator Set Manual, 00077MAN-01

[21] `www.scoliosisassociates.com/subject.php?pn=scoliosis-xray`, Scoliosis & Spines Associates, (recovered 03/03/2011)

[22] D. McRobbie, Medical Physics, **24**, #5 (1997)